

A PEM fuel cell for combined measurement of current and temperature distribution, and flow field flooding

Alex Hakenjos*, Harald Muentert, Ursula Wittstadt, Christopher Hebling

Fraunhofer Institute for Solar Energy Systems (ISE), Heidenhofstr. 2, 79110 Freiburg, Germany

Received 6 October 2003; accepted 3 November 2003

Abstract

A fuel cell has been designed that combines three methods of spatially resolved measurements. The experimental setup allows to perform a simultaneous evaluation of current, temperature and water distribution in a polymer electrolyte fuel cell (PEFC) under operation. The test cell has a segmented anode flow field for current distribution measurement. The back plate of the cathode flow field is made of an optical window, which is transparent for infrared (IR) as well as for visible wavelengths. This allows infrared thermography and optical surveillance of water droplets and flow field flooding.

© 2004 Elsevier B.V. All rights reserved.

Keywords: PEM; Fuel cell; Current distribution; Temperature distribution; Flow field flooding

1. Introduction

At present, many research activities in the field of polymer electrolyte fuel cells (PEFC) focus on the understanding of the thermodynamics as well as fluid mechanical and electrochemical processes within a fuel cell. In order to improve the fuel cell design and operation, it is necessary to learn more about the mechanisms that cause losses such as, e.g. high ionic resistance due to dry membrane conditions, low oxygen concentration in air fed fuel cell cathodes or high diffusive resistance due to flooding of the porous diffusion layer.

As most parameters that have a high influence on the different loss mechanisms (i.e. temperature, water content and gas concentration) are not distributed homogeneously over the active area of the fuel cell, measurements have to be carried out not only integrally but also spatially resolved.

One way to gather spatially resolved information of the performance and state of operation of a PEM fuel cell is the measurement of current distribution [1–4]. In combination with this method, we use infrared (IR) thermography to record the temperature distribution on the active area. Digital photography allows optical surveillance of condensed water within the flow field.

The cell which is used has a sealing system that allows to adjust and measure the clamping pressure precisely.

2. Cell design

2.1. Clamping pressure control

In order to control the clamping pressure, the anode flow field is completely separated from the MEA sealing area. It can move freely against the outer surrounding that holds an O-ring. Therefore the pressure applied to the O-ring is independent from the pressure applied to the active area. A thin flexible silicon gasket covering the end plate and the surrounding ensures gas tightness. The sealing scheme is shown in Fig. 1. The pressure is adjusted with a screw and measured with a resistive force meter between screw and flow field plate. The clamping pressure onto the active area has a strong influence on contact resistance. Therefore, it is a relevant parameter for fuel cell performance [5,6].

2.2. Current distribution measurement

For current distribution measurement the anode flow field is segmented. Forty-nine stainless steel segments (5 mm × 5 mm) have been integrated into the endplate made from plastics. Each segment is connected with a separate current line and a voltage sense. Currents are measured using a resistance multiplex method. The measurement cycle for all

* Corresponding author.

E-mail address: hakenjos@ise.fhg.de (A. Hakenjos).

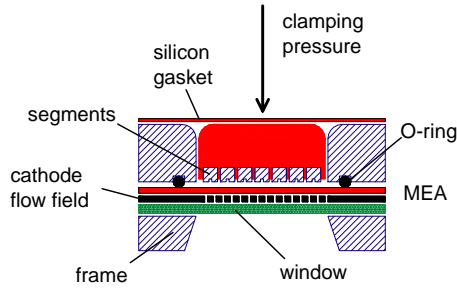


Fig. 1. Principle design of the test fuel cell.

49 segments takes about one second. The Toray carbon paper diffusion layer with a thickness of 360 μm is partially segmented as shown in Fig. 2 for lowering cross currents between adjacent segments without having to handle 49 little pieces of carbon paper. The gaps between the segments are 0.2 mm wide. The active cell area is 45 mm \times 45 mm. At the anode side the flow field is formed by square (2 mm \times 2 mm) current collector areas divided by 1 mm wide gas channels.

2.3. Temperature distribution and fluid water content measurement

The cathode flow field is machined into a graphite plate which is 2 mm thick. In this case we used a single channel meander flow field with 1 mm channel width and 1 mm wide ribs in between. The gas channels are completely broken through to allow a straight view onto the diffusion layer. Behind the flow field a zinc selenide window closes the gas channels. As zinc selenide is transparent for infrared light, we can observe the temperature of the active area with an infrared camera. The camera used is sensitive to a range of infrared wavelength between 8 and 12 μm . The transmission of the window has been tested with a fourier spectrometer.

Fig. 3 shows a transmission of about 75% over the relevant IR wavelength. The absorption of the window increases the error resulting from non ideal emission of the diffusion layer. To overcome this the temperature measurement performed with the IR camera is evaluated with an assumed effective emission coefficient. Calibration measurement are carried out with a diffusion layer electrically heated to

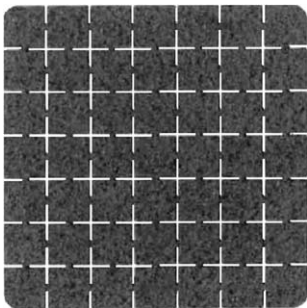


Fig. 2. Partially segmented diffusion layer for lowering cross currents between adjacent segments.

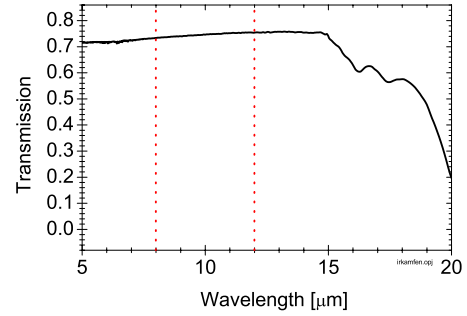


Fig. 3. Fourier spectrogram of the zinc selenide window. The IR camera is sensitive in the wavelength range between 8 and 12 μm .

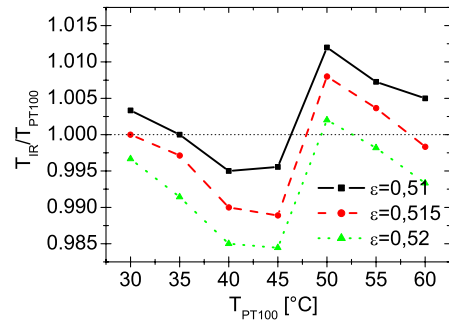


Fig. 4. Deviation of the temperatures measured with the IR camera (T_{IR}) and the PT100 (T_{PT100}). The IR measurement is evaluated assuming an error due to different effective emission coefficients ϵ .

different temperatures measured with a platinum 100 resistive sensor.

Fig. 4 shows the deviation of the IR temperature measurement evaluated with different assumed emission coefficients from the temperature measurement with the PT100. An evaluation of the IR picture assuming an effective emission coefficient of 0.515 leads to a minimal error of less than 0.3 $^{\circ}\text{C}$, i.e. 1% in the range of 30–60 $^{\circ}\text{C}$.

As the zinc selenide window is not only transparent for the IR but also for visible wavelength, it is possible to observe water droplets condensing in the gas channels. A CCD camera is used to record the flooding of the flow field.

3. Experimental

The experimental results presented in Fig. 5 have been gained under the following conditions:

- The cell was kept under constant load for 1 h before the measurement was carried out.
- The cell was driven at a constant voltage of 200 mV.
- The dry hydrogen gas flow rate was 100 sccm.
- The air was humidified to dew point temperature of 23 $^{\circ}\text{C}$.
- The air flow rate was varied from 250 to 500 and 750 sccm.

The overall current, stoichiometry, and mean temperature for different air flow rates are shown in Table 1. The rise of

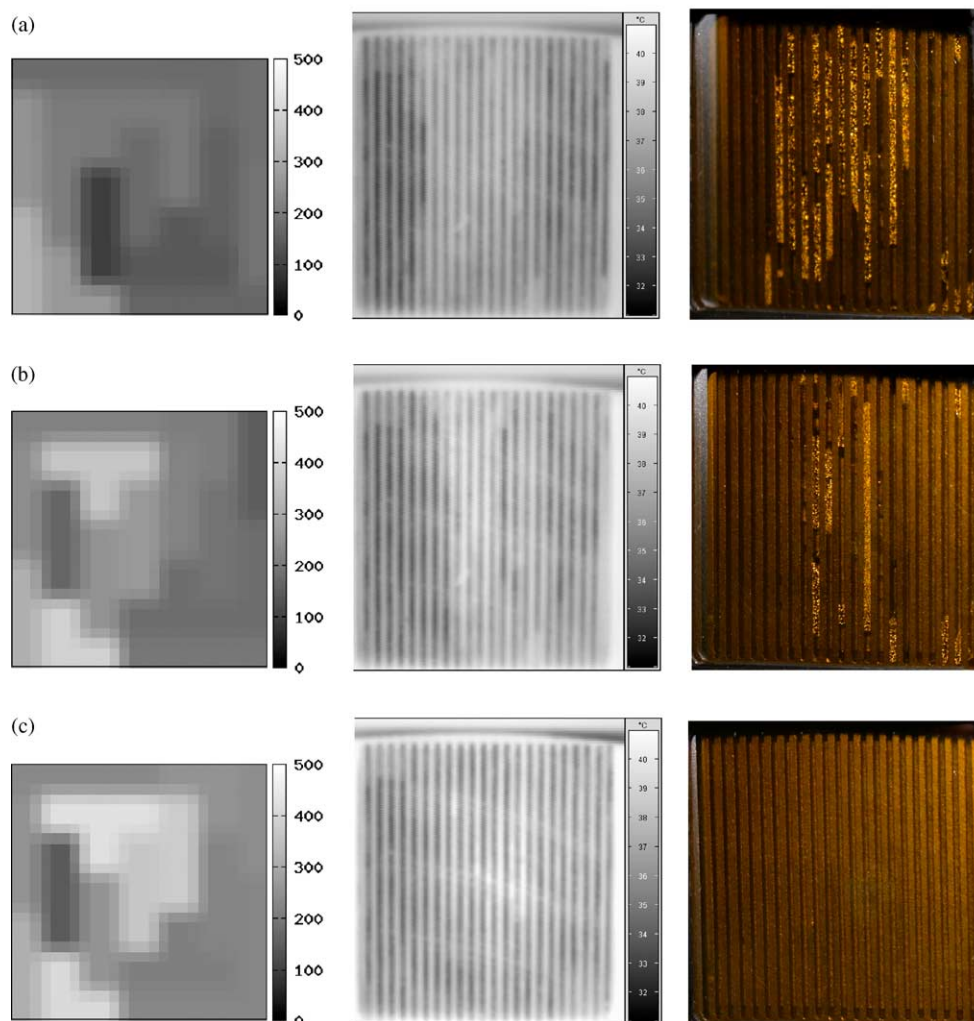


Fig. 5. Current distribution, temperature distribution and flow field flooding for air flow rates of: (a) 250 sccm; (b) 500 sccm; (c) 750 sccm. The air enters the cell in the lower left corner and the outlet is in the upper right corner. Hydrogen flows from left to right.

the cell current with rising air flow rates is explained by a higher stoichiometry and a higher water drag out of the cell. The rise of the cells mean temperature follows the rise in cell current due to reaction enthalpy.

The current and temperature distribution as well as a view on the cathode flow field for the different air flow rates are shown in Fig. 5.

At 250 sccm the CCD camera shows a large area flooded with water. This corresponds with a fairly low overall current of 3.8 A. The current distribution shows that only the inlet area is active. Looking at the temperature distribution, the

flooded area appears to be warmer even than the more active areas of the cell.

At 500 sccm the flow field flooding is restricted to almost only a small stripe in the middle of the cell. The highest current density is measured at the air inlet, but other parts of the cell are active, too. As already discussed in the case of an air flow rate of 250 sccm, the temperature measurement shows significant higher temperatures for the flooded channels.

At 750 sccm there is no water visible. The current distribution shows large areas with relatively high current density in the middle of the cell. Compared to the lower air flow rates the measurement does not show as distinct temperature differences over the whole cell area.

With no water present, we observe the same behaviour for spatially resolved measurements and overall measurements: large current densities correspond to high temperatures. This is due to the heat of reaction that occurs. As expected condensed water leads to a lower current density as the water hinders gas transport in the porous media and covers catalytic active surface. Other than expected the flooded areas

Table 1
Overall current, stoichiometry, and mean temperature for different air flow rates

Air flow rate (sccm)	Cell current (A)	Stoichiometry	Mean temperature (°C)
250	3.8	4.0	36.2
500	4.7	6.4	37.1
750	5.5	8.2	37.5

show higher temperatures in spite of lower current densities compared to the parts not flooded. A possible explanation could be a change of the emission coefficient due to the water droplets. The higher temperatures would therefore simply be caused by a systematic measurement error. But as the carbon paper is nearly black—which means a high emission coefficient—a water droplet would rather lower the emissivity. This would lead to an even lower temperature being measured. A second argument against this explanation is the rise in temperature not only in the gas channels but under the ribs as well, where no water droplet can be observed optically.

Therefore we come to the conclusion that the enthalpy of the condensing water is the cause for an elevated temperature in areas where liquid water is observed. At a temperature of around 35 °C we expect an value of 44 kJ/mol which is in the range of the heat of reaction of 15 kJ/mol. Thus heat production adds up to an almost fourfold value in areas where condensation occurs compared to dry areas at the same current density.

4. Conclusion

With the system presented current density, temperature distribution and condensed water can be observed simultaneously in a fuel cell under operation.

The combined information of the different spatially resolved measurements enables a deeper insight into fuel cell state of operation. Areas of low current density and the associated loss mechanisms can be identified. Based on this knowledge it is possible to optimise flow field design.

Here measurements for three different air flow rates are presented. Areas of flooding can be identified. The strong influence of the air flow rate on the water content is visible.

Since condensation heat has a major impact on the local temperature distribution, temperature follows the current density only in areas without liquid water formation. The experimental results can provide data for validating fuel cell simulation, especially for models that include two phase phenomena.

Acknowledgements

This work was partially sponsored by the Scholarship Programme of the German Federal Environmental Foundation DBU. Parts of the measurements have been carried out as part of a research project funded by the Federal Ministry of Education and Research.

References

- [1] S.J.C. Cleghorn, C.R. Derouin, M.S. Wilson, S. Gottesfeld, A printed circuit board approach to measuring current distribution in a fuel cell, *J. Appl. Electrochem.* 28 (1998) 663–672.
- [2] C. Wieser, A. Helmbold, E. Gülzow, A new technique for two-dimensional current distribution measurements in electrochemical cells, *J. Appl. Electrochem.* 30 (2000) 803–807.
- [3] M. Noponen, T. Mennola, M. Mikkola, T. Hottinen, P. Lund, Measurement of current distribution in a free-breathing PEMFC, *J. Power Sources* 106 (2002) 304–312. *J. Power Sources*.
- [4] D.J.L. Brett, S. Atkins, N.P. Brandon, V. Vesovic, N. Vasileiadis, A.R. Kucernak, Measurement of the current distribution along a single flow channel of a solid polymer fuel cell, *Electrochem. Commun.* (2001) 628–632.
- [5] J. Ihonen, F. Jaouen, G. Lindbergh, G. Sundholm, A novel polymer electrolyte fuel cell for laboratory investigations and in situ contact resistance measurements, *Electrochim. Acta* 46 (2001) 2899–2911.
- [6] W. Lee, C.-H. Ho, J.W. Van Zee, M. Murthy, The effects of compression and gas diffusion layers on the performance of a PEM fuel cell, *J. Power Sources* 84 (1999) 45–51.